particles

MDPI

Article

Nonholomorphic Higgsino Mass Term Effects on Muon $g-2$ and Dark Matter Relic Density in Flavor Symmetry-Based Minimal Supersymmetric Standard Model

Sajid Israr [1,†], Mario E. Gómez [2,†] and Muhammad Rehman [1,*,†]

[1] Department of Physics, COMSATS University Islamabad, Park Road, Tarlai Kalan, Islamabad 44000, Pakistan; sajidisrar7@gmail.com
[2] Department of Applied Physics, University of Huelva, 21071 Huelva, Spain; mario.gomez@dfa.uhu.es
* Correspondence: m.rehman@comsats.edu.pk
† These authors contributed equally to this work.

Abstract: We investigate the phenomenological effects of the nonholomorphic (NH) higgsino mass term, μ', within the minimal supersymmetric standard model (MSSM) extended by a non-abelian flavor symmetry, referred to as the sNHSSM. This flavor symmetry enables a substantial reduction in the number of free parameters inherent to the MSSM, streamlining them from a large set to just eight. Our study explores the interplay between cold dark matter (CDM) relic density ($\Omega_{\rm CDM}h^2$) and the anomalous magnetic moment of the muon, $(g-2)_\mu$. We study correlations among the theoretical parameters that emerge from this interplay and are further constrained by experimental data such as the Higgs boson mass, B-physics observables, and the charge and color breaking minima constraints. Moreover, our findings reveal that incorporating the NH higgsino mass term opens up new regions of parameter space that were previously inaccessible.

Keywords: dark matter relic density; nonholomorphic soft terms; anomalous magnetic moments of muon

Academic Editor: Theocharis Kosmas

Received: 1 December 2024
Revised: 12 February 2025
Accepted: 28 February 2025
Published: 6 March 2025

Citation: Israr, S.; Gómez, M. E.; Rehman, M. Nonholomorphic Higgsino Mass Term Effects on Muon $g-2$ and Dark Matter Relic Density in Flavor Symmetry-Based Minimal Supersymmetric Standard Model. *Particles* **2025**, *8*, 30. https://doi.org/10.3390/particles8010030

1. Introduction

The minimal supersymmetric standard model (MSSM) [1–6] has the potential to solve many of the lingering questions of the Standard Model (SM) [7–10] but involves over 105 free parameters, making phenomenological predictions difficult. The constrained MSSM (CMSSM) [11] reduces this to five parameters through ad hoc assumptions. However, recent findings from CMS and ATLAS have significantly constrained the CMSSM's parameter space [12]. Consequently, researchers are investigating alternative models. One such approach involves introducing non-universal Higgs masses while keeping the other scalar masses universal [13–16], a framework known as NUHM2. Another approach, which also incorporates non-universal Higgs masses, assumes that the first two generations of scalar fermions share the same mass, while the third generation can have different masses. This scenario is commonly referred to as NUHM3 [17–19]. The flavor symmetry-based MSSM (sMSSM) [20–22] presents yet another perspective, incorporating the same parameter set as NUHM3—thus introducing only two additional parameters compared to the CMSSM—but also enforcing a non-abelian flavor symmetry (H).

While the soft SUSY-breaking (SSB) sector of the MSSM generally follows the holomorphicity condition, the inclusion of nonholomorphic (NH) terms is theoretically plausible. Incorporating NH terms into the SSB sector of the MSSM introduces additional interactions

and couplings into the theory [23,24]. This can significantly impact the particle spectrum, phenomenology, and experimental observables. This enhanced framework is referred to as the nonholomorphic supersymmetric standard model (NHSSM). This approach not only expands the theoretical possibilities within supersymmetry but also offers potential solutions to discrepancies observed between MSSM predictions and experimental results [25–37]. The NHSSM can be further extended by incorporating a non-abelian flavor symmetry H, as was carried out for the MSSM. We will refer to this extended model as the sNHSSM.

One of the key advantages of the MSSM is the presence of a cold dark matter (CDM) candidate, and predicting the CDM relic density $\Omega_{\rm CDM}h^2$ in agreement with experimental measurements [38,39] has long been a goal for scientists.

Additionally, there has been growing interest in the long-standing anomaly in the $(g-2)_\mu$ measurement. The latest evaluation by the Muon $g-2$ collaboration at Fermilab [40,41], combined with earlier results from the Brookhaven E821 experiment [42], shows a 5.1σ deviation from the SM prediction [43].

However, a recent re-evaluation of isospin-breaking (IB) corrections to e^+e^- and τ-decay di-pion data [44] has narrowed the discrepancy to 2.7σ. Futhermore, when employing the latest Budapest–Marseille–Wuppertal (BMW) results for the hadronic vacuum polarization [45] and light-by-light scattering effects [46], the discrepancy is reduced to below 1σ [47].

Numerous studies in the literature have investigated the phenomenological implications of the flavor symmetry-based MSSM (sMSSM), including the $(g-2)_\mu$ anomaly and predictions for $\Omega_{\rm CDM}h^2$ [21,22,48,49]. The interplay between $\Omega_{\rm CDM}h^2$ and $(g-2)_\mu$ offers valuable insights for the MSSM [50]. Introducing nonholomorphic (NH) SSB terms expands the parameter space, potentially opening regions that were previously excluded in the MSSM [31].

This work focuses on calculating $\Omega_{\rm CDM}h^2$, $(g-2)_\mu$, and M_W within the sNHSSM framework. The primary goal is to determine whether the $(g-2)_\mu$ anomaly and $\Omega_{\rm CDM}h^2$ can be explained within the sNHSSM, and if it provides an advantage over the sMSSM.

Our analysis utilizes the tools `SARAH` [51–55], `SPheno` [56], `micrOMEGAs` [57–59], and the `SARAH Scan and Plot` (`SSP`) [60] framework. We first used `SARAH` to generate the MSSM source code for `SPheno`, enabling tasks such as spectrum generation and the calculation of low-energy observables, including $(g-2)_\mu$, B-physics observables, Δa_μ, and the W boson mass using `SPheno`. The results from `SPheno` were then fed into `micrOMEGAs` to compute the relic density of dark matter.

This paper is structured as follows: In Section 2, we outline the key features of the sNHSSM. Details of the calculations related to low-energy observables, such as $(g-2)_\mu$, are provided in Section 3. The computational framework and numerical results are discussed in Section 4, while our conclusions are presented in Section 5.

2. Flavor Symmetry-Based MSSM

2.1. SSB Sector of the MSSM

The MSSM is the simplest form of supersymmetric theories that can be built using the particle content of the SM. The complete setup for the SSB parameters is described by [1–6].

$$
\begin{aligned}
-\mathcal{L}_{\text{soft}} \;=\; & (m^2_{\tilde{Q}})^j_i \tilde{q}^{\dagger i}_L \tilde{q}_{Lj} + (m^2_{\tilde{u}})^i_j \tilde{u}^*_{Ri} \tilde{u}^j_R + (m^2_{\tilde{d}})^i_j \tilde{d}^*_{Ri} \tilde{d}^j_R \\
& + (m^2_{\tilde{L}})^j_i \tilde{l}^{\dagger i}_L \tilde{l}_{Lj} + (m^2_{\tilde{e}})^i_j \tilde{e}^*_{Ri} \tilde{e}^j_R \\
& + \tilde{m}^2_1 h^\dagger_1 h_1 + \tilde{m}^2_2 h^\dagger_2 h_2 + (B_\mu h_1 h_2 + \text{h.c.}) \\
& + (A^{ij}_d h_1 \tilde{d}^*_{Ri} \tilde{q}_{Lj} + A^{ij}_u h_2 \tilde{u}^*_{Ri} \tilde{q}_{Lj} + A^{ij}_l h_1 \tilde{e}^*_{Ri} \tilde{l}_{Lj} \\
& + \frac{1}{2} M_1 \tilde{B}_L \tilde{B}_L + \frac{1}{2} M_2 \tilde{W}^a_L \tilde{W}^a_L + \frac{1}{2} M_3 \tilde{G}^a \tilde{G}^a + \text{h.c.}). \qquad (1)
\end{aligned}
$$

Here, $m^2_{\tilde{Q}}$ and $m^2_{\tilde{L}}$ are 3×3 matrices in family space, with indices i and j representing generations, and they describe the SSB masses for the left-handed squark doublets $\tilde{q}_L$ and slepton doublets $\tilde{l}_L$ associated with $SU(2)$. Similarly, the matrices $m^2_{\tilde{u}}$, $m^2_{\tilde{d}}$, and $m^2_{\tilde{e}}$ represent the SSB masses for the right-handed up-type squarks $\tilde{u}_R$, down-type squarks $\tilde{d}_R$, and charged sleptons $\tilde{e}_R$, which are $SU(2)$ singlets. The matrices A_u, A_d, and A_l also form 3×3 matrices, corresponding to the trilinear couplings for up-type squarks, down-type squarks, and charged sleptons, respectively. The parameter μ denotes the Higgs mixing term, while $\tilde{m}_1$, $\tilde{m}_2$, and B_μ are SSB parameters related to the Higgs sector. The parameters h_1 and h_2 refer to the two Higgs doublets, and M_1, M_2, and M_3 define the mass parameters for the bino, wino, and gluino, respectively.

2.2. The Flavor Symmetry-Based NHSSM

In any supersymmetric framework, the superpotential must preserve holomorphicity, a condition that is consistently upheld when defining SSB terms within the MSSM. However, despite this traditional adherence, it is theoretically possible for NH terms to exist. In its simplest form, the SSB sector for the NH terms can be written as follows:

$$
-\mathcal{L}^{\text{NH}}_{\text{soft}} = A'^{D}_{ij} h_2 \tilde{d}^*_{Ri} \tilde{q}_{Lj} + A'^{U}_{ij} h_1 \tilde{u}^*_{Ri} \tilde{q}_{Lj} + A'^{E}_{ij} h_2 \tilde{e}^*_{Ri} \tilde{l}_{Lj} + \mu' \tilde{h}_1 \tilde{h}_2 \qquad (2)
$$

The matrices A'^{U}_{ij}, A'^{D}_{ij}, and A'^{E}_{ij} represent the NH trilinear couplings for up-type squarks, down-type squarks, and charged sleptons, respectively. The NH higgsino mass parameter μ', as introduced in Equation (2), modifies the neutralino and chargino mass matrices, which are given by

$$
\mathbf{Y} = \begin{pmatrix}
M_1 & 0 & -M_Z s_w \cos\beta & M_Z s_w \sin\beta \\
0 & M_2 & M_Z c_w \cos\beta & -M_Z c_w \sin\beta \\
-M_Z s_w \cos\beta & M_Z c_w \cos\beta & 0 & -(\mu + \mu') \\
M_Z s_w \sin\beta & -M_Z c_w \sin\beta & -(\mu + \mu') & 0
\end{pmatrix}. \qquad (3)
$$

$$
\mathbf{X} = \begin{pmatrix}
M_2 & \sqrt{2}\, M_W \sin\beta \\
\sqrt{2}\, M_W \cos\beta & (\mu + \mu')
\end{pmatrix}. \qquad (4)
$$

Although the NH trilinear couplings may influence the couplings of the SUSY particles, the NH parameter μ' does not affect the couplings of the SUSY particle, but rather only modifies the neutralino and chargino mass matrices. This characteristic renders it particularly significant for observables involving neutralinos and charginos, such as $\Omega_{\text{CDM}} h^2$. In our current investigation, the NH trilinear couplings hold less relevance, while the interplay between μ and μ' emerges as potentially crucial.

2.3. Flavor Symmetry-Based NHSSM

Equation (1) contains over 105 free parameters, making it difficult to produce viable phenomenological predictions in the MSSM. However, in the CMSSM, this large number of

parameters is drastically reduced to just five by assuming that scalar masses and gaugino masses are unified at the GUT scale. Despite the drastic reduction in the number of parameters, experimental results from the LHC have severely constrained the CMSSM parameter space. To overcome the limitations of the CMSSM, a class of supersymmetric models has been developed where the SSB Lagrangian is defined purely by symmetry considerations. This framework, known as the flavor symmetry-based MSSM (sMSSM), imposes two key symmetry conditions on the SSB Lagrangian. First, the parameters respect a grand unified symmetry, such as $\mathtt{SO}(10)$, and second, a non-abelian flavor symmetry H acts on the three particle generations, suppressing Flavor-Changing Neutral Currents (FCNCs) mediated by SUSY particles. Specific examples of these models [61–65] are constructed with flavor symmetries like $\mathtt{SU}(2)_H$ and $\mathtt{SO}(3)_H$, where the generations transform as $\mathbf{2}+\mathbf{1}$ and $\mathbf{3}$ representations, respectively. In $\mathtt{SU}(2)_H$, flavor-violating D-terms are suppressed using an interchange symmetry, while the $\mathtt{SO}(3)_H$ framework naturally avoids D-term problems. In this context, it is sufficient to group the first two generations in a multiplet to resolve the SUSY flavor problem, with the third family treated as a singlet. Hence, both $\mathbf{2}+\mathbf{1}$ and $\mathbf{3}$ assignments are valid.

Compatibility with $\mathtt{SO}(10)$ offers significant advantages for SSB, reducing the soft masses for sfermions from fifteen (under the SM gauge symmetry) to just three [20], lowering the number of free parameters. It also provides a symmetry-based reason for gaugino mass unification, cutting the free parameters from three to one. The sMSSM adds two more free parameters compared to the CMSSM, bringing the total to seven. The resulting parameter space is equivalent to that of NUHM3; hence, the forthcoming analysis is equally relevant to the NUHM3 model. The concept of flavor symmetry can also be incorporated into the NHSSM framework to reduce the number of input parameters. By setting the NH trilinear couplings to zero or equal to the holomorphic trilinear couplings, the only additional parameter in the model would be μ'. Thus, the input parameters in the sNHSSM will comprise the following:

$$\{m_{0_{1,2}}, m_{0_3}, M_{1/2}, A_0, \tan\beta, \mu, m_A, \mu'\}.$$

where $m_{0_{1,2}}$ represents the SSB mass parameter for the first two families of sfermions, m_{0_3} for the third generation, $M_{1/2}$ for the SSB gaugino mass, and A_0 for the SSB trilinear coupling. The parameters $\tan\beta$ and M_A represent the ratio of the vacuum expectation values of the two Higgs doublets and the mass of the $\mathcal{CP}$-odd Higgs boson A, respectively.

3. Calculation of Low-Energy Observables

SUSY Contributions to $(g-2)_\mu$

As mentioned earlier, the discrepancy between the current world average (WA) SM predictions [43,66] and CDF measurements stands at 5.1σ, given by

$$\Delta a_\mu^{\mathrm{WA}} = a_\mu^{\mathrm{exp}} - a_\mu^{\mathrm{SM,\,WA}} = (24.9 \pm 4.8) \times 10^{-10}. \tag{5}$$

Similarly, for IB corrections, we have

$$\Delta a_\mu^{\mathrm{IB}} = a_\mu^{\mathrm{exp}} - a_\mu^{\mathrm{SM,\,IB}} = (14.8^{+5.1}_{-5.4}) \times 10^{-10}, \tag{6}$$

while the BMW results yield

$$\Delta a_\mu^{\mathrm{BMW}} = a_\mu^{\mathrm{exp}} - a_\mu^{\mathrm{SM,\,BMW}} = (0.4 \pm 4.2) \times 10^{-10}. \tag{7}$$

The value of $\Delta a_\mu^{\text{BMW}}$ aligns with zero, suggesting no significant deviation between the SM prediction and experimental measurements, thereby leaving minimal scope for new physics effects. On the other hand, $\Delta a_\mu^{\text{BMW}}$ demands moderate contributions from beyond the SM physics, while Δa_μ^{WA} points to even larger contributions. This underscores the unresolved nature of the $(g-2)_\mu$ anomaly. Nevertheless, a comprehensive exploration of potential new physics contributions to $(g-2)_\mu$ could shed light on this anomaly and delineate the relevant parameter space for such theories.

This discrepancy can be addressed by incorporating the MSSM contributions to $(g-2)_\mu$. The primary MSSM contributions stem from loops involving sleptons, charginos, and neutralinos, as illustrated in Figure 1. The corrections from the Feynman diagrams shown in Figure 1 can be summarized as in [67–70].

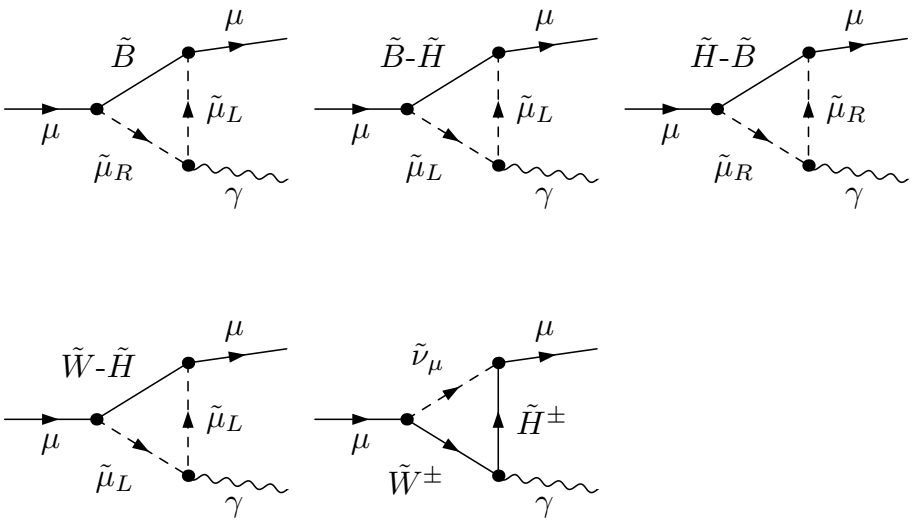

Figure 1. Feynman diagrams for dominant MSSM contributions to $(g-2)_\mu$ originating from different neutralino and chargino species. The diagrams shown as ($\tilde{B}$-$\tilde{H}$), ($\tilde{H}$-$\tilde{B}$), and ($\tilde{W}$-$\tilde{H}$) represent mixing between neutralino species.

$$\Delta a_\mu^{\text{MSSM}} = \Delta a_\mu^{\tilde{B}\tilde{\mu}_L\tilde{\mu}_R} + \Delta a_\mu^{(\tilde{B}-\tilde{H})\tilde{\mu}_L} + \Delta a_\mu^{(\tilde{H}-\tilde{B})\tilde{\mu}_R} + \Delta a_\mu^{(\tilde{H}-\tilde{W})\tilde{\mu}_L} + \Delta a_\mu^{(\tilde{W}-\tilde{H})\tilde{\nu}_\mu} \tag{8}$$

where

$$\Delta a_\mu^{\tilde{B}\tilde{\mu}_L\tilde{\mu}_R} = \frac{g_Y^2}{8\pi^2}\frac{m_\mu^2 \mu \tan\beta}{M_1^3} F_b\left(\frac{m_{\tilde{\mu}_L}^2}{M_1^2}, \frac{m_{\tilde{\mu}_R}^2}{M_1^2}\right) \tag{9}$$

$$\Delta a_\mu^{(\tilde{H}-\tilde{B})\tilde{\mu}_R} = \frac{-g_Y^2}{8\pi^2}\frac{m_\mu^2 M_1 \mu \tan\beta}{m_{\tilde{\mu}_R}^4} F_b\left(\frac{M_1^2}{m_{\tilde{\mu}_R}^2}, \frac{\mu^2}{m_{\tilde{\mu}_R}^2}\right) \tag{10}$$

$$\Delta a_\mu^{(\tilde{B}-\tilde{H})\tilde{\mu}_L} = \frac{g_Y^2}{16\pi^2}\frac{m_\mu^2 M_1 \mu \tan\beta}{m_{\tilde{\mu}_L}^4} F_b\left(\frac{M_1^2}{m_{\tilde{\mu}_L}^2}, \frac{\mu^2}{m_{\tilde{\mu}_L}^2}\right) \tag{11}$$

$$\Delta a_\mu^{(\tilde{H}-\tilde{W})\tilde{\mu}_L} = \frac{-g^2}{16\pi^2}\frac{m_\mu^2 M_2 \mu \tan\beta}{m_{\tilde{\mu}_L}^4} F_b\left(\frac{M_2^2}{m_{\tilde{\mu}_L}^2}, \frac{\mu^2}{m_{\tilde{\mu}_L}^2}\right) \tag{12}$$

$$\Delta a_\mu^{(\tilde{W}-\tilde{H})\tilde{\nu}_\mu} = \frac{g^2}{8\pi^2}\frac{m_\mu^2 M_2 \mu \tan\beta}{m_{\tilde{\nu}_\mu}^4} F_a\left(\frac{M_2^2}{m_{\tilde{\nu}_\mu}^2}, \frac{\mu^2}{m_{\tilde{\nu}_\mu}^2}\right) \tag{13}$$

with $F_a(x,y)$ and $F_b(x,y)$ defined as

$$F_a(x,y) = \frac{-1}{2(x-y)}\left(\frac{(x-1)(x-3)+2\ln x}{(x-1)^3} - \frac{(y-1)(y-3)+2\ln y}{(y-1)^3}\right)$$
$$F_b(x,y) = \frac{-1}{2(x-y)}\left(\frac{(x-1)(x+1)-2x\ln x}{(x-1)^3} - \frac{(y-1)(y+1)-2y\ln y}{(y-1)^3}\right)$$

As can be seen from Equations (9)–(13), all the contributions are proportional to $\mu\tan\beta$; however, the value of $\mu\tan\beta$ is constrained by the vacuum stability bounds and electroweak symmetry breaking (EWSB).

4. Numerical Results

4.1. Computational Strategy

The workflow for our computation is outlined as follows. Using the Mathematica package `SARAH` [51–55], we first generated the NHSSM source code for `SPheno` [56]. `SPheno` is a tool that performs numerical calculations of SUSY mass spectra, particle decay rates, and various low-energy observables such as Δa_μ. Similarly, we used `SARAH` to generate the `micrOMEGAs` [57–59] source code, enabling us to include dark matter constraints in our analysis. These codes were interfaced with `SSP` [60], a Mathematica package that streamlines parameter scans and data visualization. The following parameter set was employed for random scans within the sNHSSM framework:

$$\begin{array}{rcl} 0 \leq & m_{0_{1,2}} & \leq 5 \text{ TeV} \\ 0 \leq & m_{0_3} & \leq 15 \text{ TeV} \\ 0 \leq & M_{1/2} & \leq 2 \text{ TeV} \\ -3 \leq & A_0/m_{0_3} & \leq 3 \text{ TeV} \\ 0 \leq & M_A & \leq 10 \text{ TeV} \\ 1 \leq & \tan\beta & \leq 60. \end{array}$$

We set the NH trilinear terms to zero. Additionally, in conjunction with the previously specified parameter ranges, we applied the following ranges for μ and μ':

$$\begin{array}{rcl} 0 \leq & \mu & \leq 600 \text{ GeV} \\ 0 \leq & \mu' & \leq 600 \text{ GeV} \end{array}$$

These specified boundary conditions were applied at the GUT scale, except for the parameters μ, μ', and M_A, which were defined at the SUSY scale instead. Additionally, a custom code was implemented within the `SSP` package to calculate the constraints related to charge- and color-breaking minima (CCB), based on Refs. [33,71]. Data were then generated in accordance with the following constraints on low-energy observables:

$$\begin{array}{c} M_h = 123 - -127 \text{ GeV}, \\ m_{\tilde{g}} \geq 2.1 \text{ TeV}, \\ 1.99\times10^{-9} \leq \text{BR}(B_s \to \mu^+\mu^-) \leq 3.43\times10^{-9}\ (2\sigma), \\ 3.02\times10^{-4} \leq \text{BR}(B \to X_s\gamma) \leq 3.62\times10^{-4}\ (2\sigma), \\ 0.115 \leq \Omega_{\text{CDM}}h^2 \leq 0.125\ (5\sigma). \end{array}$$

The current theoretical uncertainty in MSSM predictions for M_h is approximately 1.5 GeV [72]. However, we chose a range of 123 GeV $\leq M_h \leq$ 127 GeV. For M_W, we selected the 2σ range of M_W^{avg}. The values for $\text{BR}(B \to X_s\gamma)$ and $\text{BR}(B_s \to \mu^+\mu^-)$ were also set at the 2σ level of their experimentally measured values [73,74]. The lower limit on Ω_{CDM} can be overlooked, as other particle species may contribute to the dark matter

relic abundance. Consequently, we focus solely on points that are consistent with the LSP neutralino relic density, ensuring it aligns with or is lower than the Planck measurements [75]. Nonetheless, we explore the parameter space where both upper and lower limits can be satisfied.

4.2. Δa_μ and $\Omega_{\rm CDM}h^2$ in the sNHSSM

In a previous study [49], we investigated the $(g-2)_\mu$ discrepancy and $\Omega_{\rm CDM}h^2$ within the framework of the sMSSM. We carefully examined the most suitable parameter space, revealing correlations between the input parameters and the various constraints, which we reproduce here for completeness:

$$\begin{array}{ccc} 0 \leq & m_{0_{1,2}} & \leq 3 \text{ TeV} \\ 7 \leq & m_{0_3} & \leq 15 \text{ TeV} \\ 0.8 \leq & M_{1/2} & \leq 2 \text{ TeV} \\ 0 \leq & \mu & \leq 570 \text{ GeV} \end{array}$$

The constraints on $m_{0_{1,2}}$ and μ arise from considerations related to $\Delta a_\mu^{\rm WA}$, while those on m_{0_3} and $M_{1/2}$ are derived from M_h and $m_{\tilde{g}}$, respectively.

The addition of nonholomorphic SSB terms in the MSSM offers rich phenomenology. The μ' term, in particular, can have very important consequences. As already mentioned, the μ' term does not affect the couplings of the sparticles but only the mass matrices of the neutralinos and charginos. This, in turn, has the potential to significantly change $\Omega_{\rm CDM}h^2$ while leaving other phenomenological aspects unchanged. We have specifically checked that the constraints and correlations between the parameters described above are not affected by the inclusion of μ'.

As we said above, the inclusion of μ' affects mainly the chargino and neutralino masses; therefore, we find similar values for the other SUSY masses and parameters to the ones presented in Ref. [49]. According to those results, the relic density bounds are satisfied by neutralinos with a sizeable higgsino component; then, LSP composition and coanihilations with charginos will change with the new parameter μ', leading to interesting results when both terms are below 600 GeV.

The impact of the new parameter can be seen in Figure 2, where we present the NHSSM predictions in the M_A-μ plane. The purple $+$ and cyan $\times$ markers represent parameter points within the 2σ range of $\Delta a_\mu^{\rm IB}$ and $\Delta a_\mu^{\rm WA}$, respectively. Points with predictions below the IB bounds are not shown, despite being compatible with the BMW constraints. All displayed points respect the upper 5σ constraint of the Planck limit, but only the green dots satisfy the lower bound as well. Hence, only the green points can explain the Planck results, while for the remaining points, additional DM components are required. To indicate the models that can simultaneously accommodate both DM constraints and provide a solution to the $(g-2)_\mu$ problem, we mark with black (red) stars the points that satisfy the 2σ range of $\Delta a_\mu^{\rm IB}$ ($\Delta a_\mu^{\rm WA}$) while also ensuring that $\Omega_{\rm CDM}h^2$ remains within 5σ of the Planck limit. In Ref. [49], it was shown that the 5σ range of $\Omega_{\rm CDM}h^2$ prefers $\mu > 600\,$GeV, while $\Delta a_\mu^{\rm WA}$ favors values of μ below 450 GeV. Consequently, there are only very narrow regions where both constraints can be simultaneously satisfied. Notably, most of the cyan $\times$ lie in the region where $\mu \leq 450$ GeV, as before. However, after the inclusion of μ', the green points can now be found in the region where $\mu < 450$ GeV. The additional contribution to $\Omega_{\rm CDM}h^2$ comes from the presence of μ' in the neutralino and chargino mass matrices, making it easier to explain the $\Delta a_\mu^{\rm WA}$ discrepancy while still adhering to the upper and lower limits for $\Omega_{\rm CDM}h^2$. This can be seen by the presence of black and red stars that satisfy the 2σ range of $\Delta a_\mu^{\rm IB}$ and $\Delta a_\mu^{\rm WA}$ while also ensuring that $\Omega_{\rm CDM}h^2$ remains within 5σ of the Planck limit.

It is worth noting that these constraints become less stringent when considering $\Delta a_\mu^{\rm IB}$, which permits smaller values of $\Delta a_\mu^{\rm NHSSM}$. Furthermore, since $\Delta a_\mu^{\rm BMW}$ is compatible with zero discrepancy, it allows the parameter space to extend to even higher values of μ.

In Figure 3, we show the NHSSM predictions in the $\mu' - \mu$ plane. The color coding remains the same as in the previous figure. We can see that lower values of μ and μ' favor $\Delta a_\mu^{\rm WA}$ prediction at 2σ, while the opposite applies to the 5σ range of $\Omega_{\rm CDM}h^2$. Points satisfying $\Delta a_\mu^{\rm IB}$ ($\Delta a_\mu^{\rm WA}$) and $\Omega_{\rm CDM}h^2$ constraints, shown as black (red) stars, are found along one of the diagonals of the plot. As we said before, the main effect of the inclusion of μ' arises from the shifting of the masses of neutralinos and charginos. This is significant in our model because the 5σ range of $\Omega_{\rm CDM}h^2$ is reached mainly in cases where the LSP neutralino has a significant higgsino component together with a moderate degeneracy with the NLSP chargino, as was shown in Ref. [49]. Indeed, in Figure 3 we can see that inclusion of μ' increases the number of models with relic density inside Planck range, while lower values explain better the $\Delta a_\mu^{\rm WA}$ anomaly. However, the overlapping regions satisfying both limits are significantly increased with respect to the area found in Ref. [49]. In addition, in Figure 4 we can see that the range of masses for the LSP is similar to that found in the former reference. However, models with lower values of μ predict LSPs with large scattering cross-sections with nucleons. Therefore, as we will see in the next section, models that can explain DM predict spin-independent cross-sections that have already been excluded by direct detection experiments.

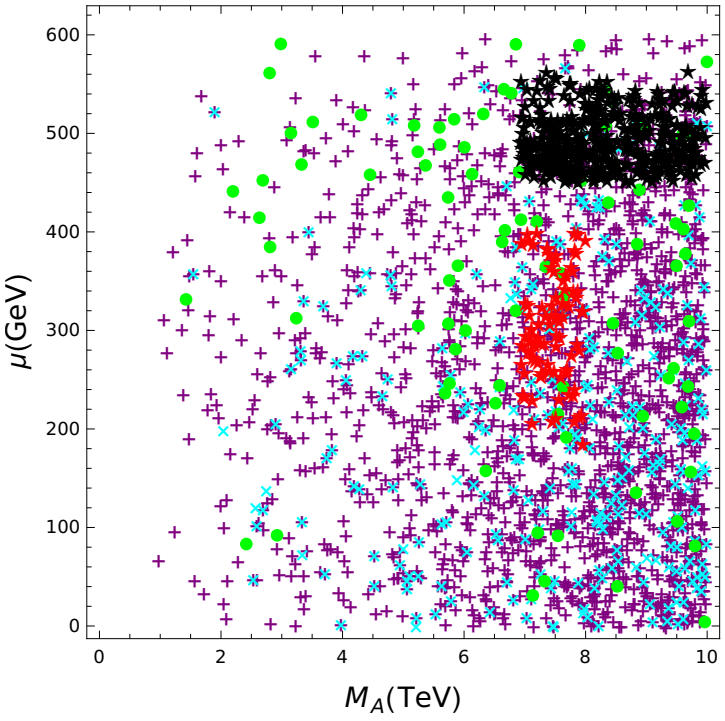

Figure 2. NHSSM predictions in the M_A-μ plane. The purple $+$ and cyan $\times$ markers represent parameter points within the 2σ range of $\Delta a_\mu^{\rm IB}$ and $\Delta a_\mu^{\rm WA}$, respectively. Green dots indicate points that satisfy the 5σ constraint of the Planck limit. Black (red) stars denote points that satisfy the 2σ range of $\Delta a_\mu^{\rm IB}$ ($\Delta a_\mu^{\rm WA}$) while also ensuring that $\Omega_{\rm CDM}h^2$ remains within 5σ of the Planck limit.

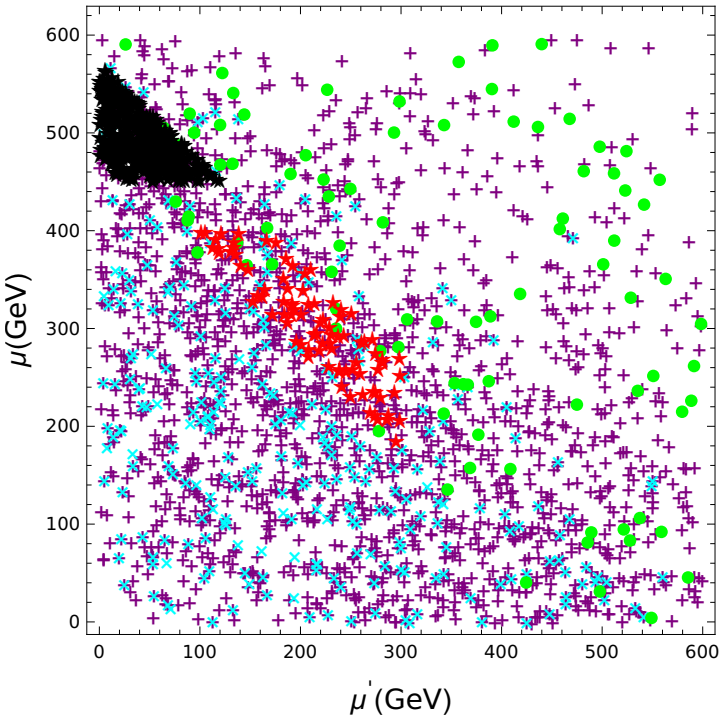

Figure 3. NHSSM predictions in the μ'-μ plane. The purple + and cyan × markers represent parameter points within the 2σ range of $\Delta a_\mu^{\rm IB}$ and $\Delta a_\mu^{\rm WA}$, respectively. Green dots indicate points that satisfy the 5σ constraint of the Planck limit. Black (red) stars denote points that satisfy the 2σ range of $\Delta a_\mu^{\rm IB}$ ($\Delta a_\mu^{\rm WA}$) while also ensuring that $\Omega_{\rm CDM}h^2$ remains within 5σ of the Planck limit.

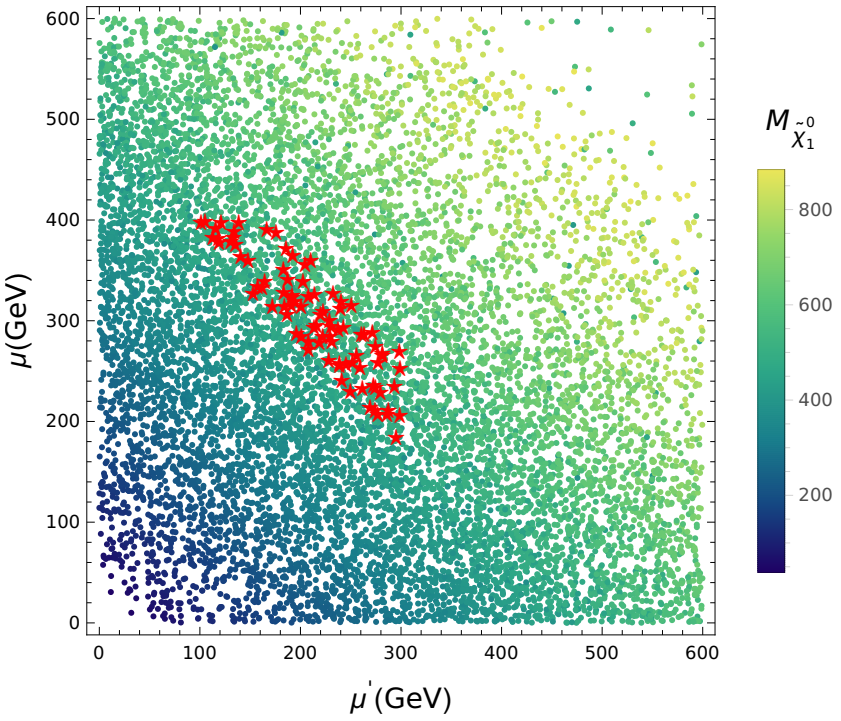

Figure 4. $M_{\tilde{\chi}_1^0}$ shown in the μ'-μ plane. The color bar indicates the values of $M_{\tilde{\chi}_1^0}$, whereas the red stars are the locations that simultaneously satisfy the $\Delta a_\mu^{\rm WA}$, and $\Omega_{\rm CDM}h^2$ constraints.

4.3. Spin-Independent WIMP–Proton Cross-Section Constraints

As we mentioned in the previous section, the LSP predicted in the framework under consideration is a well-tempered mixture of bino and higgsino. Therefore, the WIMP–nucleon cross-section can reach significant values. In Figure 5, we present

our results for the spin-independent WIMP–proton cross-section, $\sigma^p_{\rm SI}$ (pb), as a function of the lightest neutralino mass, $M_{\tilde{\chi}^0_1}$. We also present the current direct detection constraints from the XENONnt (dashed blue), LUX (orange), and future projections from the DARWIN (dashed purple) experiments. The left panel includes a color bar representing the values of $\Omega_{\rm CDM}h^2$, while the right panel highlights parameter points satisfying the 2σ constraints of $\Delta a_\mu^{\rm IB}$ (purple +) and $\Delta a_\mu^{\rm WA}$ (cyan $\times$). We scale $\sigma^p_{\rm SI}$ by a factor of $\Omega_{\rm CDM}h^2/0.114$ to account for the possibility that additional particle species may contribute to the total DM relic density.

From the left panel, it is evident that almost all parameter points satisfying Planck's 5σ limits on $\Omega_{\rm CDM}h^2$ are already excluded by the constraints from LUX and XENON experiments. This suggests that the model remains viable only if the lower bound on $\Omega_{\rm CDM}h^2$ is relaxed. Meanwhile, the right panel shows that viable regions still exist where the 2σ constraints of $\Delta a_\mu^{\rm BMW}$, $\Delta a_\mu^{\rm IB}$, and $\Delta a_\mu^{\rm WA}$ are simultaneously satisfied. However, it should be kept in mind that $\Delta a_\mu^{\rm BMW}$ is compatible with zero, opening up a region of parameter space. These points correspond to those with Δa_μ below the IB region, which are not shown in Figure 5.

Finally, in Table 1, we present three benchmark points, all of which satisfy the constraints from M_h, M_W, and the direct detection limits set by LUX. We also show the range for scalar quark mass eigenstates, denoted by $m_{\tilde{u}_1}$–$m_{\tilde{u}_6}$. The first point, P_1, falls within the 2σ range of $\Delta a_\mu^{\rm WA}$, but the predicted value of $\Omega_{\rm CDM}h^2$ remains very low. In this case, both μ and μ' are small, whereas $\tan\beta$ is considerably high. Similarly, the second point, P_2, lies within the 2σ range of $\Delta a_\mu^{\rm IB}$, yet $\Omega_{\rm CDM}h^2$ remains significantly lower than the Planck value. Here, μ and μ' are relatively large, while $\tan\beta$ remains moderate. The third point, P_3, predicts $\Omega_{\rm CDM}h^2$ within the 5σ range; however, the $(g-2)\mu$ value is very small and is only compatible with $\Delta a_\mu^{\rm BMW}$.

Table 1. Three benchmark points in the sNHSSM that satisfy the M_h, M_W, and $\sigma^p_{\rm SI}$ constraints, along with their corresponding predictions for key observables.

Parameter	P_1	P_2	P_3
$m_{0_{1,2}}$	2.245 TeV	0.852 TeV	1.833 TeV
m_{0_3}	10.9422 TeV	11.309 TeV	9.701 TeV
$M_{1/2}$	968.671 GeV	1845 GeV	1117.45 GeV
$\tan\beta$	59.66	42.39	34.45
A_0	-0.194 GeV	0.254 GeV	-0.273 GeV
M_A	7.964 TeV	8.214 TeV	1.425 TeV
μ	15.66 GeV	300.0 GeV	331.45 GeV
μ'	71.12 GeV	564.2 GeV	528.48 GeV
$m_{\tilde{u}_1}$–$m_{\tilde{u}_6}$	1.285–7.562 TeV	3.064–9.379 TeV	2.541–8.160 TeV
M_h	124.153 GeV	123.67 GeV	123.66 GeV
M_W	80.402 GeV	80.405 GeV	80.400 GeV
$\Delta a_\mu^{\rm NHSSM}$	27.0×10^{-10}	5.20×10^{-10}	1.56×10^{-10}
$\Omega_{\rm CDM}h^2$	0.004	0.008	0.117
$\sigma^p_{\rm SI}$ (pb) $\times\,\Omega_{\rm CDM}h^2/0.114$	1.99×10^{-11}	9.78×10^{-11}	8.04×10^{-11}

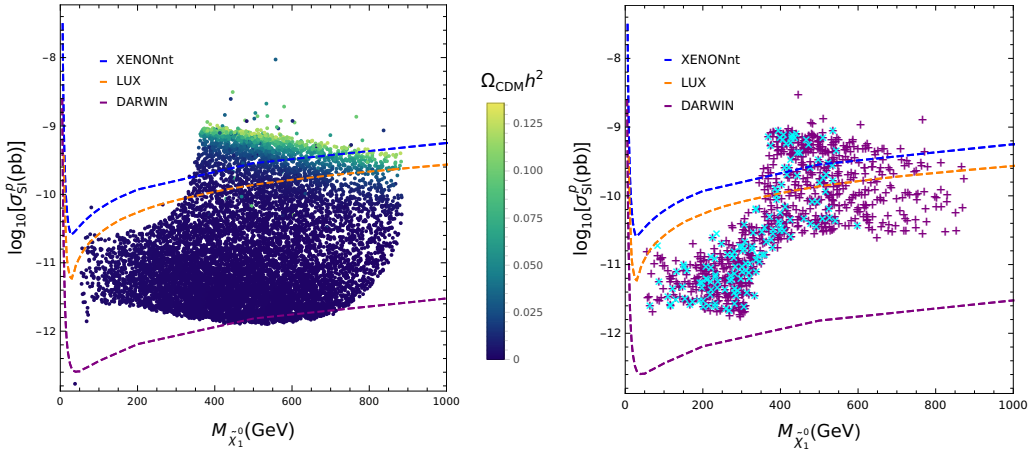

Figure 5. The $\log_{10}(\sigma^p_{\rm SI}\,({\rm pb}))$ is presented as a function of $M_{\tilde{\chi}^0_1}$, along with the current direct detection constraints from XENONnt (dashed blue), LUX (orange), and future projections from DARWIN (dashed purple) experiments. In the left plot, the color bar represents the values of $\Omega_{\rm CDM}h^2$, while in the right plot, purple + and cyan $\times$ indicate parameter points satisfying the 2σ range of $\Delta a_\mu^{\rm IB}$, and $\Delta a_\mu^{\rm WA}$, respectively.

5. Conclusions

The flavor symmetry-based minimal supersymmetric standard model (sMSSM) is proposed as an alternative to the constrained MSSM (CMSSM), which encounters difficulties aligning with LHC data. This model uses non-abelian flavor symmetry at the GUT scale to reduce free parameters to seven. Extending the sMSSM by adding a nonholomorphic (NH) soft SUSY-breaking term μ' increases the input parameters to eight, forming the sNHSSM.

In this paper, we examine predictions for the muon's anomalous magnetic moment $(g-2)_\mu$ and dark matter relic density $\Omega_{\rm CDM}h^2$ in the sNHSSM. We generated the NHSSM source code for `SPheno` and `micrOMEGAs` using the Mathematica package `SARAH`, and then used the `SSP` setup for particle spectra and low-energy observable calculations, including M_h, M_W, Δa_μ, and $\Omega_{\rm CDM}h^2$. Our parameter scans respect constraints from the Higgs boson mass M_h, B-physics observables, experimental gluino mass limits, and dark matter relic density bounds.

We found values for μ lower than those in the case of the sMSSM, which allows for a larger number of models predicting $\Omega_{\rm CDM}h^2$ within the 5σ range, while also predicting a sizeable contribution to $\Delta a_\mu^{\rm NHSSM}$. However, these models tend to predict WIMPs excluded by direct detection, so the only points predicting $\sigma^p_{\rm SI}$ below the LUX bounds are those compatible with the SM BMW evaluation of the $(g-2)_\mu$, which does not require a significant contribution from physics beyond the SM. For instance, we provide three benchmarks with the relevant physical observables in scenarios where the $\Delta a_\mu^{\rm NHSSM}$ range is computed according to three different evaluations of the deviation from the SM.

Author Contributions: Conceptualization, S.I. and M.R.; Validation, S.I.; Formal analysis, S.I.; Writing—original draft, M.R.; Writing—review & editing, M.E.G.; Supervision, M.E.G. and M.R. All authors have read and agreed to the published version of the manuscript.

Funding: The research of M.E.G. is supported by the Spanish MICINN, under grant PID2022-140440NB-C22. The research of M.R. is supported by the Pakistan Higher Education Commission (HEC), under NRPU grant Ref No. 20-15867/NRPU/R&D/HEC/2021.

Data Availability Statement: The original contributions presented in this study are included in the article. Further inquiries can be directed to the corresponding author(s).

Conflicts of Interest: The authors have no competing interests to declare that are relevant to the content of this article.

References

1. Fayet, P. Supergauge Invariant Extension of the Higgs Mechanism and a Model for the electron and Its Neutrino. *Nucl. Phys. B* **1975**, *90*, 104–124. [CrossRef]
2. Fayet, P. Supersymmetry and Weak, Electromagnetic and Strong Interactions. *Phys. Lett. B* **1976**, *64*, 159. [CrossRef]
3. Fayet, P. Spontaneously Broken Supersymmetric Theories of Weak, Electromagnetic and Strong Interactions. *Phys. Lett. B* **1977**, *69*, 489. [CrossRef]
4. Nilles, H.P. Supersymmetry, Supergravity and Particle Physics. *Phys. Rept.* **1984**, *110*, 1–162. [CrossRef]
5. Haber, H.E.; Kane, G.L. The Search for Supersymmetry: Probing Physics Beyond the Standard Model. *Phys. Rept.* **1985**, *117*, 75–263. [CrossRef]
6. Barbieri, R. Looking Beyond the Standard Model: The Supersymmetric Option. *Riv. Nuovo Cim.* **1988**, *11N4*, 1–45. [CrossRef]
7. Glashow, S.L. Partial Symmetries of Weak Interactions. *Nucl. Phys.* **1961**, *22*, 579–588. [CrossRef]
8. Weinberg, S. A Model of Leptons. *Phys. Rev. Lett.* **1967**, *19*, 1264–1266. [CrossRef]
9. Salam, A. Weak and Electromagnetic Interactions. *Conf. Proc. C* **1968**, *680519*, 367–377. [CrossRef]
10. Glashow, S.L.; Iliopoulos, J.; Maiani, L. Weak Interactions with Lepton-Hadron Symmetry. *Phys. Rev. D* **1970**, *2*, 1285–1292. [CrossRef]
11. Kane, G.L.; Kolda, C.F.; Roszkowski, L.; Wells, J.D. Study of constrained minimal supersymmetry. *Phys. Rev. D* **1994**, *49*, 6173–6210. [CrossRef] [PubMed]
12. Sekmen, S. Highlights on Supersymmetry and Exotic Searches at the LHC. In Proceedings of the 32nd Rencontres de Blois on Particle Physics and Cosmology, Blois, France, 17–22 October 2022; Volume 4.
13. Matalliotakis, D.; Nilles, H.P. Implications of nonuniversality of soft terms in supersymmetric grand unified theories. *Nucl. Phys. B* **1995**, *435*, 115–128. [CrossRef]
14. Olechowski, M.; Pokorski, S. Electroweak symmetry breaking with nonuniversal scalar soft terms and large tan beta solutions. *Phys. Lett. B* **1995**, *344*, 201–210. [CrossRef]
15. Polonsky, N.; Pomarol, A. Nonuniversal GUT corrections to the soft terms and their implications in supergravity models. *Phys. Rev. D* **1995**, *51*, 6532–6549. [CrossRef] [PubMed]
16. Nath, P.; Arnowitt, R.L. Nonuniversal soft SUSY breaking and dark matter. *Phys. Rev. D* **1997**, *56*, 2820–2832. [CrossRef]
17. Ellis, J.R.; Olive, K.A.; Santoso, Y. The MSSM parameter space with nonuniversal Higgs masses. *Phys. Lett. B* **2002**, *539*, 107–118. [CrossRef]
18. Ellis, J.R.; Falk, T.; Olive, K.A.; Santoso, Y. Exploration of the MSSM with nonuniversal Higgs masses. *Nucl. Phys. B* **2003**, *652*, 259–347. [CrossRef]
19. Baer, H.; Mustafayev, A.; Profumo, S.; Belyaev, A.; Tata, X. Direct, indirect and collider detection of neutralino dark matter in SUSY models with non-universal Higgs masses. *J. High Energy Phys.* **2005**, *7*, 65. [CrossRef]
20. Babu, K.S.; Gogoladze, I.; Raza, S.; Shafi, Q. Flavor Symmetry Based MSSM (sMSSM): Theoretical Models and Phenomenological Analysis. *Phys. Rev. D* **2014**, *90*, 056001.
21. Babu, K.S.; Gogoladze, I.; Shafi, Q.; Ün, C.S. Muon $g-2$, 125 GeV Higgs boson, and neutralino dark matter in a flavor symmetry-based MSSM. *Phys. Rev. D* **2014**, *90*, 116002.
22. Babu, K.S.; Gogoladze, I.; Un, C.S. Proton lifetime in minimal SUSY SU(5) in light of LHC results. *J. High Energy Phys.* **2022**, *2*, 164.
23. Girardello, L.; Grisaru, M.T. Soft Breaking of Supersymmetry. *Nucl. Phys. B* **1982**, *194*, 65. [CrossRef]
24. Bagger, J.; Poppitz, E. Destabilizing divergences in supergravity coupled supersymmetric theories. *Phys. Rev. Lett.* **1993**, *71*, 2380–2382. [CrossRef] [PubMed]
25. Jack, I.; Jones, D.R.T. Nonstandard soft supersymmetry breaking. *Phys. Lett. B* **1999**, *457*, 101–108. [CrossRef]
26. Jack, I.; Jones, D.R.T. Quasiinfrared fixed points and renormalization group invariant trajectories for nonholomorphic soft supersymmetry breaking. *Phys. Rev. D* **2000**, *61*, 095002. [CrossRef]
27. Cakir, M.A.; Mutlu, S.; Solmaz, L. Phenomenological issues in supersymmetry with non-holomorphic soft breaking. *Phys. Rev. D* **2005**, *71*, 115005. [CrossRef]
28. Ün, C.S.; Tanyıldızı, C.H.; Kerman, S.; Solmaz, L. Generalized Soft Breaking Leverage for the MSSM. *Phys. Rev. D* **2015**, *91*, 105033.
29. Chattopadhyay, U.; Dey, A. Probing Non-holomorphic MSSM via precision constraints, dark matter and LHC data. *J. High Energy Phys.* **2016**, *10*, 27.
30. Chattopadhyay, U.; Das, D.; Mukherjee, S. Exploring Non-Holomorphic Soft Terms in the Framework of Gauge Mediated Supersymmetry Breaking. *J. High Energy Phys.* **2018**, *2018*, 158.
31. Un, C.S. Low fine-tuning with heavy higgsinos in Yukawa unified SUSY GUTs. *Turk. J. Phys.* **2024**, *48*, 1–27.

32. Chattopadhyay, U.; Datta, A.; Mukherjee, S.; Swain, A.K. Sbottoms as probes to MSSM with nonholomorphic soft interactions. *J. High Energy Phys.* **2018**, *10*, 202.
33. Chattopadhyay, U.; Das, D.; Mukherjee, S. Probing Lepton Flavor Violating decays in MSSM with Non-Holomorphic Soft Terms. *J. High Energy Phys.* **2020**, *6*, 15.
34. Chattopadhyay, U.; Datta, A.; Mukherjee, S.; Swain, A.K. Associated production of heavy Higgs bosons with a $b\bar{b}$ pair in the nonholomorphic MSSM and LHC searches. *J. High Energy Phys.* **2022**, *8*, 113.
35. Rehman, M.; Heinemeyer, S. Nonholomorphic soft-term contributions to the Higgs-boson masses in the Feynman diagrammatic approach. *Phys. Rev. D* **2023**, *107*, 095033.
36. Israr, S.; Rehman, M. Higgs Decay to $Z\gamma$ in the Minimal Supersymmetric Standard Model and Its Nonholomorphic Extension *arXiv* **2024**, arXiv:2407.01210.
37. Rehman, M.; Heinemeyer, S. Lepton Flavor Violation in Nonholomorphic Soft SUSY-Breaking Scenarios: Experimental Limits and Excesses. *arXiv* **2024**, arXiv:2411.00479.
38. Goldberg, H. Constraint on the Photino Mass from Cosmology. *Phys. Rev. Lett.* **1983**, *50*, 1419. . Erratum in *Phys. Rev. Lett.* **2009**, *103*, 099905. [CrossRef]
39. Ellis, J.R.; Hagelin, J.S.; Nanopoulos, D.V.; Olive, K.A.; Srednicki, M. Supersymmetric Relics from the Big Bang. *Nucl. Phys. B* **1984**, *238*, 453–476. [CrossRef]
40. Aguillard, D.P.; Albahri, T.; Allspach, D.; Anisenkov, A.; Badgley, K.; Baeßler, S.; Bailey, I.; Bailey, L.; Baranov, V.A.; Barlas-Yucel, E.; et al. Measurement of the Positive Muon Anomalous Magnetic Moment to 0.20 ppm. *Phys. Rev. Lett.* **2023**, *131*, 161802,
41. Abi, B.; Albahri, T.; Al-Kilani, S.; Allspach, D.; Alonzi, L.P.; Anastasi, A.; Anisenkov, A.; Azfar, F.; Badgley, K.; Baeßler, S.; et al. Measurement of the Positive Muon Anomalous Magnetic Moment to 0.46 ppm. *Phys. Rev. Lett.* **2021**, *126*, 141801.
42. Bennett, G.W.; Bousquet, B.; Brown, H.N.; Bunce, G.; Carey, R.M.; Cushman, P.; Danby, G.T.; Debevec, P.T.; Deile1, M.; Deng, H.; et al. Final Report of the Muon E821 Anomalous Magnetic Moment Measurement at BNL. *Phys. Rev. D* **2006**, *73*, 072003. [CrossRef]
43. Aoyama, T.; Asmussen, N.; Benayoun, M.; Bijnens, J.; Blum, T.; Bruno, M.; Caprini, I.; Calame, C.C.; Cè, M.; Colangelo, G.; et al. The anomalous magnetic moment of the muon in the Standard Model. *Phys. Rept.* **2020**, *887*, 1–166. [CrossRef]
44. Miranda, A. Compatibility between e^+e^- and τ decay data in the di-pion channel and implications for a_μ^{SM} and CVC tests. In Proceedings of the 10th International Conference on Quarks and Nuclear Physics, Barcelona, Spain, 8–12 July 2024; Volume 11.
45. Boccaletti, A.; Borsanyi, S.; Davier, M.; Fodor, Z.; Frech, F.; Gerardin, A.; Giusti, D.; Kotov, A.Y.; Lellouch, L.; Lippert, T.; et al. High precision calculation of the hadronic vacuum polarisation contribution to the muon anomaly. *arXiv* **2024**, arXiv:2407.10913.
46. Fodor, Z.; Gerardin, A.; Lellouch, L.; Szabo, K.K.; Toth, B.C.; Zimmermann, C. Hadronic light-by-light scattering contribution to the anomalous magnetic moment of the muon at the physical pion mass. *arXiv* **2024**, arXiv:2411.11719.
47. Coutinho, A.M.; Karan, A.; Miralles, V.; Pich, A. Light scalars within the $\mathcal{CP}$-conserving Aligned-two-Higgs-doublet model. *arXiv* **2024**, arXiv:2412.14906v2 . [CrossRef]
48. Hussain, M.; Khalid, R. Understanding the muon anomalous magnetic moment in light of a flavor symmetry-based Minimal Supersymmetric Standard Model. *Prog. Theor. Exp. Phys.* **2018**, *2018*, 083B06.
49. Israr, S.; Gomez, M.E.; Rehman, M.; Arafat, Y. Interplay between M_W, $\Omega_{\mathrm{CDM}}h^2$, and $(g-2)_\mu$ in Flavor Symmetry-Based Supersymmetric Models. *arXiv* **2024**, arXiv:2410.09719.
50. Bagnaschi, E.; Chakraborti, M.; Heinemeyer, S.; Saha, I.; Weiglein, G. Interdependence of the new "MUON G-2" result and the W-boson mass. *Eur. Phys. J. C* **2022**, *82*, 474.
51. Staub, F. From Superpotential to Model Files for FeynArts and CalcHep/CompHep. *Comput. Phys. Commun.* **2010**, *181*, 1077–1086.
52. Staub, F. Automatic Calculation of supersymmetric Renormalization Group Equations and Self Energies. *Comput. Phys. Commun.* **2011**, *182*, 808–833.
53. Staub, F. SARAH 3.2: Dirac Gauginos, UFO output, and more. *Comput. Phys. Commun.* **2013**, *184*, 1792–1809.
54. Staub, F. SARAH 4: A tool for (not only SUSY) model builders. *Comput. Phys. Commun.* **2014**, *185*, 1773–1790.
55. Staub, F. Exploring new models in all detail with SARAH. *Adv. High Energy Phys.* **2015**, *2015*, 840780.
56. Porod, W. SPheno, a program for calculating supersymmetric spectra, SUSY particle decays and SUSY particle production at e^+ e^- colliders. *Comput. Phys. Commun.* **2003**, *153*, 275–315.
57. Belanger, G.; Boudjema, F.; Pukhov, A.; Semenov, A. MicrOMEGAs 2.0: A Program to calculate the relic density of dark matter in a generic model. *Comput. Phys. Commun.* **2007**, *176*, 367–382.
58. Belanger, G.; Boudjema, F.; Pukhov, A.; Semenov, A. micrOMEGAs_3: A program for calculating dark matter observables. *Comput. Phys. Commun.* **2014**, *185*, 960–985.
59. Barducci, D.; Belanger, G.; Bernon, J.; Boudjema, F.; Da Silva, J.; Kraml, S.; Laa, U.; Pukhov, A. Collider limits on new physics within micrOMEGAs_4.3. *Comput. Phys. Commun.* **2018**, *222*, 327–338.

60. Staub, F.; Ohl, T.; Porod, W.; Speckner, C. A Tool Box for Implementing Supersymmetric Models. *Comput. Phys. Commun.* **2012**, *183*, 2165–2206.
61. Dine, M.; Leigh, R.G.; Kagan, A. Flavor symmetries and the problem of squark degeneracy. *Phys. Rev. D* **1993**, *48*, 4269–4274.
62. Barbieri, R.; Dvali, G.R.; Hall, L.J. Predictions from a U(2) flavor symmetry in supersymmetric theories. *Phys. Lett. B* **1996**, *377*, 76–82.
63. Chen, M.C.; Mahanthappa, K.T. CP violation in a supersymmetric SO(10) x U(2)(F) model. *Phys. Rev. D* **2002**, *65*, 053010.
64. King, S.F.; Ross, G.G. Fermion masses and mixing angles from SU (3) family symmetry and unification. *Phys. Lett. B* **2003**, *574*, 239–252.
65. Ross, G.G.; Velasco-Sevilla, L.; Vives, O. Spontaneous CP violation and nonAbelian family symmetry in SUSY. *Nucl. Phys. B* **2004**, *692*, 50–82.
66. Martin, S.P.; Wells, J.D. Muon Anomalous Magnetic Dipole Moment in Supersymmetric Theories. *Phys. Rev. D* **2001**, *64*, 035003.
67. Moroi, T. The Muon anomalous magnetic dipole moment in the minimal supersymmetric standard model. *Phys. Rev. D* **1996**, *53*, 6565–6575; Erratum in *Phys. Rev. D* **1997**, *56*, 4424. [CrossRef] [PubMed]
68. Stockinger, D. The Muon Magnetic Moment and Supersymmetry. *J. Phys. G* **2007**, *34*, R45–R92.
69. Fargnoli, H.; Gnendiger, C.; Paßehr, S.; Stöckinger, D.; Stöckinger-Kim, H. Two-loop corrections to the muon magnetic moment from fermion/sfermion loops in the MSSM: Detailed results. *J. High Energy Phys.* **2014**, *2*, 70.
70. Cho, G.C.; Hagiwara, K.; Matsumoto, Y.; Nomura, D. The MSSM confronts the precision electroweak data and the muon $g-2$. *J. High Energy Phys.* **2011**, *11*, 68.
71. Beuria, J.; Dey, A. Exploring Charge and Color Breaking vacuum in Non-Holomorphic MSSM. *J. High Energy Phys.* **2017**, *10*, 154.
72. Slavich, P.; Heinemeyer, S.; Bagnaschi, E.; Bahl, H.; Goodsell, M.; Haber, H.E.; Hahn, T.; Harlander, R.; Hollik, W.; Lee, G.; et al. Higgs-mass predictions in the MSSM and beyond. *Eur. Phys. J. C* **2021**, *81*, 450.
73. Particle Data Group; Workman, R.L.; Burkert, V.D.; Crede, V.; Klempt, E.; Thoma, U.; Tiator, L.; Agashe, K.; Aielli, G.; Allanach, B.C.; et al. Review of Particle Physics. *Prog. Theor. Exp. Phys.* **2022**, *2022*, 083C01. [CrossRef]
74. ATLAS, CMS and LHCb Collaborations. Combination of the ATLAS, CMS and LHCb Results on the $B^0_{(s)} \to \mu^+\mu^-$ Decays. ATLAS-CONF-2020-049. 2020. Available online: https://cds.cern.ch/record/2727216 (accessed on 26 November 2024).
75. Aghanim, N.; Akrami, Y.; Ashdown, M.; Aumont, J.; Baccigalupi, C.; Ballardini, M.; Banday, A.J.; Barreiro, R.B.; Bartolo, N.; Basak, S.; et al. Planck 2018 results. VI. Cosmological parameters. *Astron. Astrophys.* **2020**, *641*, A6; Erratum in *Astron. Astrophys.* **2021**, *652*, C4. [CrossRef]